LBL-17012

CONF-8305109--3

Lawrence Berkeley Laboratory
UNIVERSITY OF CALIFORNIA

LBL--17012

DE84 006615

Presented at the VII Nobel Conference: "The Metabolism of the Human Brain Studied with Positron Emission Tomography", Saltsjöbaden, Sweden, May 17-20, 1983; and to be published in the Proceedings

DETECTORS FOR HIGH RESOLUTION DYNAMIC PET

S.E. Derenzo, T.F. Budinger, and R.H.Huesman

May 1983

Biology & Medicine Division

Prepared for the U.S. Department of Energy under Contract DE-AC03-76SF00098

DETECTORS FOR HIGH RESOLUTION DYNAMIC PET*

S.E. Derenzo, T.F. Budinger, and R.H. Huesman

Donner Laboratory and Lawrence Berkeley Laboratory
University of California
Berkeley, CA 94720

ABSTRACT

This report reviews the motivation for high spatial resolution in dynamic positron emission tomography of the head and the technical problems in realizing this objective. We present recent progress in using small silicon photodiodes to measure the energy deposited by 511 keV photons in small BGO crystals with an energy resolution of 9.4% full-width at half-maximum. In conjunction with a suitable phototube coupled to a group of crystals, the photodiode signal to noise ratio is sufficient for the identification of individual crystals both for conventional and time-of-flight positron tomography.

Presented at the VII Nobel Conference: "The Metabolism of the Human Brain Studied with Positron Emission Tomography", May 17-20, 1983, Saltsjöbaden, Sweden

To be published in: The Metabolism of the Human Brain Studied with Positron Emission Tomography, L. Widén, Editor, Raven Press, New York, 1984

*This work was supported in part by the Director, Office of Energy Research, Office of Health and Environmental Research of the U.S. Department of Energy, under Contract No. DE-AC03-76SF00098, and in part by the National Institutes of Health, National Heart, Lung, and Blood Institute under grant No. P01 HL25840.

1. MEDICAL OBJECTIVES AND TOMOGRAPH DESIGN PHILOSOPHY

In positron emission tomography of the brain, a spatial resolution of 2 mm full-width at half-maximum (FWHM) is needed to measure tracer flow in vascular spaces and the uptake and clearance of tracers in small structures (Figure 1). Moreover, improved resolution in positron tomography results in more accurate quantitation by reducing smearing from one region to another. A high resolution image with the same number of events as a low resolution image will appear noisier, but the placement of reconstructed activity will more accurately reflect the true distribution. This accuracy is compromised with the low resolution image, no matter how many events are taken (Figure 2). A second reason for improving resolution is to aid visual discrimination of activity in closely adjacent structures with differing physiological functions.

To achieve high spatial resolution while retaining good temporal resolution and detection efficiency, our tomograph design philosophy incorporates the following factors:

(1) Multiple rings of closely packed detector crystals of high density and atomic number for good detection efficiency

(2) Small crystals for good spatial resolution (< 2 mm FWHM in plane, < 5 mm FWHM axial)

(3) A minimum of detector sampling motion (stationary or two-position clam) for short imaging times (< 2 sec)

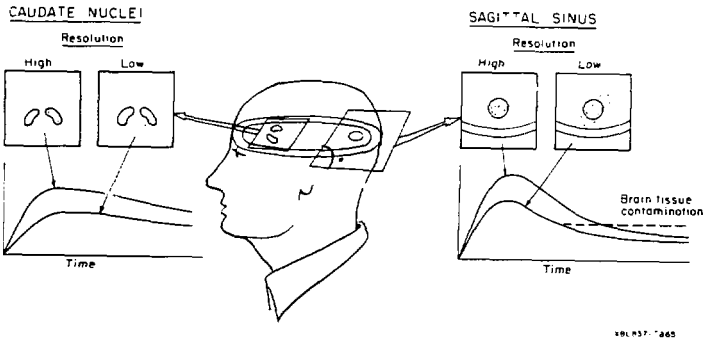

Figure 1: A spatial resolution < 2 mm FWHM and a data acquisition time < 2 sec is required for accurate, dynamic quantitation of blood pool activity (sagittal sinus) and of brain tissue activity (e.g. caudate nuclei).

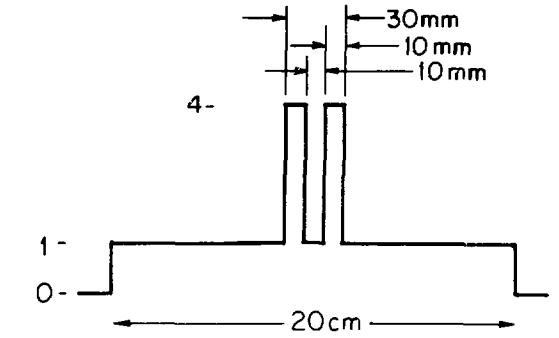

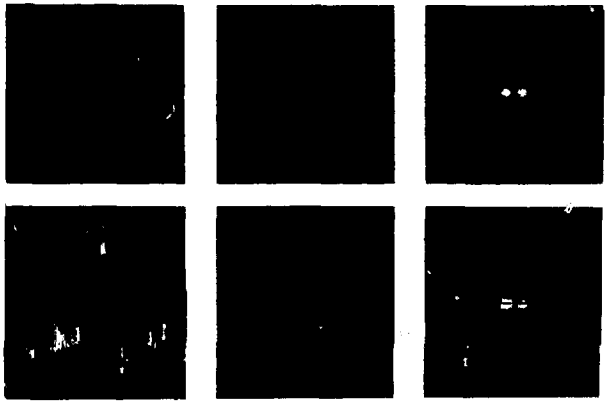

XBB 836-4730

Figure 2: Simulated reconstructions of 3 x 10^6 events from a 20 cm diam disc of activity with two 10 mm diam circular regions containing an activity concentration four times higher than the disc. Quantitative accuracy is excellent for 2.5 mm crystals (left), good for 5 mm crystals (center), and poor for 10 mm crystals (right).

(4) Many parallel detector channels for low deadtime and high rates

(5) Photopeak pulse height selection on each crystal for rejection of tissue-scattered annihilation photons and multiple crystal interactions

(6) Good timing resolution (3 to 10 nsec full coincidence window) for accidental background rejection

(7) Optimal shielding design for the rejection of prompt scatter and accidental backgrounds

These design factors are discussed in detail in References [1-7].

2. LIMITS TO SPATIAL RESOLUTION IN PET

(1) POSITRON RANGE

The effect of positron range on spatial resolution has been reported for several isotopes by several workers [8,9]. By using the Donner 280-Crystal positron tomograph, we imaged thin positron sources in polyurethane foam to measure the distribution of positron annihilation points for ^{18}F, ^{11}C, ^{68}Ga, and ^{82}Rb [10]. Although these distributions are sharply peaked and have narrow FWHM and standard deviation (rms) values, most of the annihilations are in the extensive tails, as evidenced by the diameter of the circle that contains 75% of the projected annihilation points (Table 1). The sharp peaking permits derivation of a range deconvolution kernel that can correct for range effects with a loss in signal-to-noise ratio that depends on the positron energy and projection bin size. If this kernel is combined with the reconstruction kernel, then the range deconvolution can be performed during the reconstruction with no additional computational effort.

TABLE 1. Positron range in water

Isotope	^{18}F	^{11}C	^{68}Ga	^{82}Rb
Maximum Energy	0.64 MeV	0.96 MeV	1.90 MeV	3.35 MeV
PSF FWHM[a]	0.13 mm	0.13 mm	0.31 mm	0.42 mm
PSF rms[b]	0.23 mm	0.39 mm	1.2 mm	2.6 mm
Diameter (75%)[c]	1.2 mm	2.1 mm	5.4 mm	12.4 mm

[a]Full-width at half-maximum of projected point spread function
[b]Root-mean-square deviation from center of projected point spread function
[c]Diameter of circle containing 75% of the projected annihilations

(2) DEVIATIONS FROM 180° EMISSION

The positron-electron pair has a random residual energy of typically 10 eV at the instant of annihilation. The resulting angular deviations from 180° emission have a nearly Gaussian distribution with FWHM = 5.7 mrad as measured in water at 20°C [11]. For a detector ring diameter of 60 cm (appropriate for a head tomograph), this results in a positional uncertainty of 0.9 mm FWHM at the center of the system.

(3) DETECTOR SIZE AND DETECTION EFFICIENCY

If a point source of positrons is placed midway between opposing coincident detectors of width W, and moved orthogonal to the line between the detectors, their geometrical response will be a triangular function with FWHM = W/2. The advantage of using smaller detectors to improve this component of spatial resolution is offset, however, by a lower efficiency due to the reduced probability of interacting in a single crystal (Table 2).

TABLE 2. Detection Efficiency of BGO and BaF_2 crystals for 511 keV photons as a function of width

Crystal Width	Threshold	BGO Efficiency[a]	BaF_2 Efficiency[b]
1 mm	100 keV[c]	61%	48%
	photopeak[d]	51%	22%
2 mm	100 keV	67%	52%
	photopeak	56%	25%
3 mm	100 keV	70%	54%
	photopeak	59%	27%
5 mm	100 keV	75%	58%
	photopeak	64%	29%
10 mm	100 keV	80%	65%
	photopeak	69%	34%
20 mm	100 keV	84%	69%
	photopeak	72%	38%

[a] $Bi_4Ge_3O_{12}$ Crystal height 10 mm, depth 30 mm
[b] BaF_2 Crystal height 10 mm, depth 50 mm
[c] Single crystal interactions with >100 keV absorption
[d] Single crystal interactions with full 511 keV absorption

(4) LINEAR SAMPLING DENSITY

For detectors of width W, the geometrical resolution W/2 discussed above will not be realized in the reconstructed image unless the effective tomographic sampling distance is W/4 or finer throughout the image region. The stationary circular tomograph samples every W/2, providing the best possible temporal resolution, but at some sacrifice in spatial resolution. Although arbitrarily fine sampling can be achieved by using a large number of sufficiently small crystals, this is technically more difficult and more expensive if the crystals are to be read out individually. As a result, mechanical motion of the detectors is employed. The most commonly used sampling motion is the circular "wobble", which can provide excellent sampling but typically involves 8 or more positions [12-14]. The need for short imaging times limits the number of mechanical positions that can be used to achieve this sampling density. The "clam" sampling motion provides W/4 sampling uniformly in angle with only two mechanical positions [15].

(5) PENETRATION FOR OFF-AXIS SOURCES

Detector penetration for off-axis sources causes a radial elongation of the reconstructed point spread function. This is a smaller effect for BGO than for NaI(Tl), CsF, or BaF_2.

(6) MULTIPLE CRYSTAL INTERACTIONS

For systems that use small crystals and do not measure the energy absorbed in each crystal, Compton scattering in one crystal followed by an interaction in a nearby crystal occurs frequently and is a source of position error. For example, using the Monte Carlo computer code described in Reference [16], we calculate that a linear array of 3 mm x 10 mm x 30 mm deep BGO crystals has a gross detection efficiency (any absorption in any crystal) of 93%, a photopeak detection efficiency (full 511 keV absorption in one or more crystals) of 76%, but a single-crystal photopeak efficiency (full 511 keV absorption in one crystal) of only 59%. Thus 22% of the photopeak events are the result of multiple crystal interactions. For 3 mm x 10 mm x 50 mm deep BaF_2 crystals, the gross detection efficiency is 88%, the 100 keV efficiency (a total absorption of $\geq$ 100 keV among one or more crystals) is 78% and the single-crystal 100 keV efficiency is 53%. Thus 32% of the $\geq$ 100 keV events are the result of multiple crystal interactions. In contrast, most of these confusing events are rejected by systems that can provide two pulse height thresholds for each crystal (e.g. T_1 = 50 keV, T_2 = 450 keV), and require that one crystal be above T_2 while all nearby crystals are below T_1.

(7) RECONSTRUCTION FILTER

The process of reconstructing the projection data taken by the detector array will generally smooth the resulting image to an extent determined by the reconstruction filter [17]. Other workers have advocated using a filter that smooths the statistical fluctuations of the data during the reconstruction with the intention of improving the appearance of the image, but this causes a smearing of data from one region to the next. Our philosophy has been to use a filter that achieves nearly the resolution of the tomograph. Activity in a region of interest is determined by summing the values of the individual picture elements comprising that region. This approach improves quantitation and averages over statistical fluctuations without artificially introducing

contributions from nearby picture elements.

3. DETECTOR DESIGNS FOR HIGH SPATIAL RESOLUTION PET

The primary restriction in constructing a multi-ring positron tomograph with small, close-packed, individually coupled crystals is the size of available phototubes. It is very difficult to build phototubes for close-packed crystals narrower than 6 mm, because the thickness of the glass walls limits the area of active photocathode. At the present time, the two smallest phototubes are the cylindrical Hamamatsu R1635 (10 mm diameter) and the rectangular Hamamatsu R1770 (6 mm x 24 mm).

One solution to the problem of dead space taken by the glass walls is to incorporate many small electron multipliers and anodes within a single glass envelope. A quadrant phototube [18] and a dual phototube [19] have been reported. The development of a new phototube with < 3 mm wide electron multiplier structures is a substantial undertaking with significant financial risk. The microchannel phototube can accomplish this objective, but more development is necessary to improve its useful lifetime and packing fraction.

Several economical coding schemes have been developed for coupling small, close-packed crystals to larger phototubes [20-22]. In these approaches each phototube receives light from several crystals, and deadtime and multiple crystal interactions are of special concern. Using a new modification of Anger position logic, Burnham et al. [20] have achieved a detector resolution of 4 mm FWHM.

A promising new approach uses a high-quality rectangular PMT coupled to a group of crystals for timing information and a solid state photodetector individually coupled to each crystal for identification [6,23-25]. Using the Monte Carlo computer code described in Reference [26], we find that the light collected by a silicon photodiode and a phototube coupled to the same BGO crystal is largest when the phototube and photodiode are coupled to the full areas of orthogonal faces of the crystal (Figure 3).

4. PREVIOUS WORK WITH BGO CRYSTALS AND SOLID STATE PHOTOSENSORS

The first report of the use of photodiodes to read out BGO for the detection of individual charged particles estimated an energy resolution of 2-3 MeV FWHM [27]. More recently, two types of low-capacitance, low dark current silicon photodiodes have been developed by the Hamamatsu TV Co. of Japan in collaboration with D. Groom of the University of Utah. Using a BGO crystal and the Hamamatsu S1723 silicon photodiode with 10 mm x 10 mm sensitive area and a reverse-biased capacitance of 70 pF, Groom measured an energy resolution of 750 keV FWHM [28].

Using a 3 mm x 10 mm x 2 mm deep BGO crystal coupled to a 3 mm x 10 mm HgI_2 crystal used as a photodetector, Iwanczyk and co-workers measured a 511 keV photopeak resolution of 19% FWHM [29]. Since HgI_2 is an insulator (band gap 2.2 eV), it can be used in thick layers to provide very low capacitance and low dark current. Unfortunately, the HgI_2 photodetector is not yet commercially available.

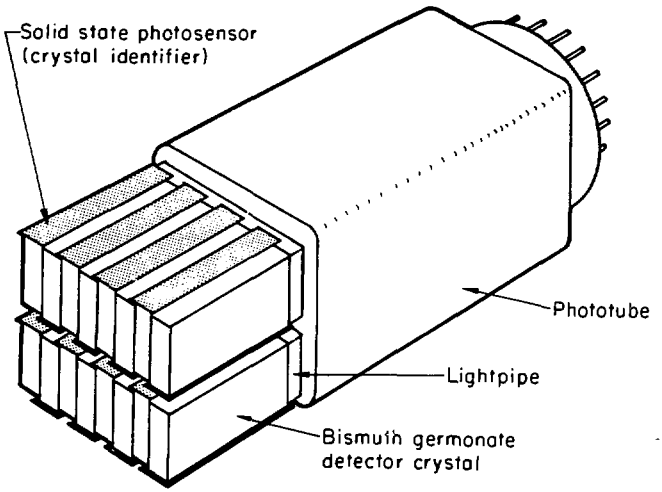

XBL8212-4298

Figure 3: Schematic of a multiple-crystal array mounted on a single phototube for coincident timing information. Crystal identification (and measurement of the energy deposited in each crystal) is provided by individually coupled silicon photodiodes.

5. SUMMARY OF TEST RESULTS USING BGO CRYSTALS AND SILICON PHOTODIODES

To investigate how well silicon photodiodes could detect BGO scintillation flashes, we used the Hamamatsu S1722 silicon photodiode, which has a 4 mm diam sensitive area and a reverse-biased capacitance of 12 pF. A 3 x 3 x 3 mm^3 BGO crystal was selected that had a 662 keV photopeak resolution of 12% FWHM measured by a Hamamatsu R1306 bialkali phototube. The photodiode was cemented to the crystal, connected to a negative bias supply and grounded through a low-noise charge amplifier (Figure 4). The BGO crystal, photodiode, and amplifier front end were mounted in a metal container that could be maintained at temperatures from +20°C to -190°C with liquid nitrogen. The subsequent shaping amplifier was kept at room temperature and consisted of a simple RC integrator and RC differentiator.

At 20°C and 10 V reverse bias, the dark current was approximately 3 nA, the best pulse peaking time was 2 μsec, and the 662 keV photopeak produced 3200 e^- and had 27% FWHM (Figure 5a). Cooling decreased the dark current and amplifier noise while increasing the BGO signal. Using a peaking time of 1 μsec, the best temperature was -75°C and the 662 keV photopeak had 20% FWHM (Figure 5b). The best 662 keV photopeak resolution we observed was 7.2% FWHM using a temperature of -150°C and an amplifier peaking time of 10 μsec (Figure 5c). The improvement from Figure 5a to 5c is the result of a 2.4-fold increase in signal and a 1.9-fold decrease in noise. Table 3 lists the pulse height resolution for gamma rays of various energy. These results are described in

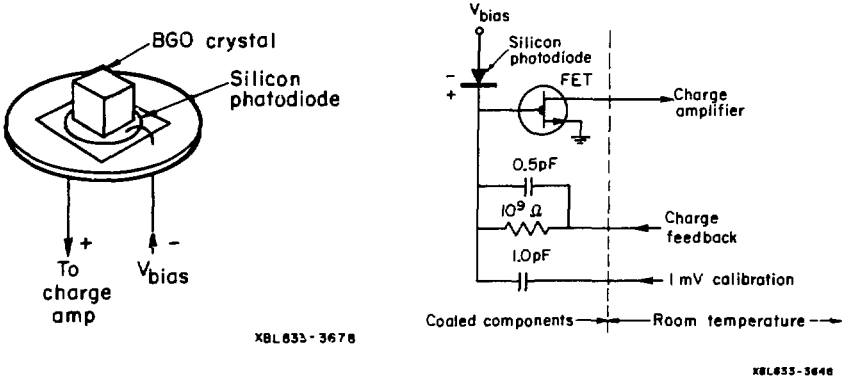

Figure 4: (a) Schematic of 3 x 3 x 3 mm^3 BGO crystal mounted on a Hamamatsu R1722-01 silicon photodiode with 4 mm diameter photosensitive area. Crystal was polished, cemented to photodiode with RTV and coated with MgO powder. (b) Schematic of cooled components of the scintillator, photodiode and charge amplifier.

more detail in reference [24].

6. CONCLUSIONS

(1) High resolution (<2 mm FWHM), efficient, dynamic positron emission tomography is needed to measure tracer flow in vascular spaces and the uptake and clearance of tracers in small structures of the brain.

(2) Positron range and deviations from 180^{o} emission impose a fundamental resolution limit of about 1-2 mm FWHM. This limit is not reached in existing tomograph designs due to detector resolution.

(3) Silicon photodiodes can measure the scintillation light of small (< 5 mm) BGO crystals with better pulse height resolution than previously reported photodetectors, but electronic noise makes timing accuracy poor. One way to overcome this limitation is to use silicon photodiodes coupled individually for crystal identification and pulse height information, and photomultipliers coupled to groups of crystals for timing information. The photodiode signal to noise ratio observed in this work is sufficient for the identification of individual crystals both for conventional and time-of-flight positron tomography.

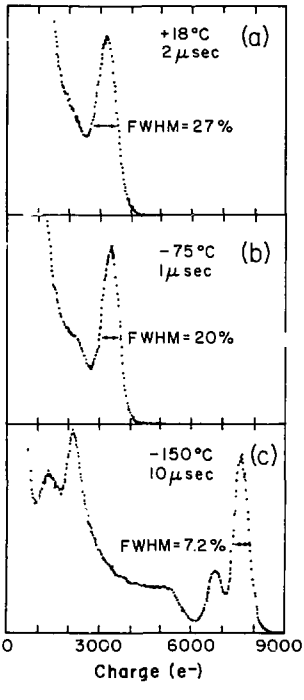

Figure 5: Pulse height spectrum for 662 keV gamma rays using the set-up of Figure 4. (a) Optimal amplifier peaking time τ = 2 μsec at a fixed temperature of +18°C. (b) Optimal temperature of -75°C at a fixed amplifier peaking time of τ = 1 μsec. (c) Overall optimal resolution at τ = 10 μsec, and -150°C.

ACKNOWLEDGEMENTS

We thank T. Vuletich for invaluable technical assistance, B. Baringer and T. Ortiz for assistance in data taking, N. Servies and A. Kurahashi of Hamamatsu, Corp. for providing silicon photodiodes, and M. Cavalli-Sforza, J. Cahoon, F. Goulding, D. Groom, and D. Landis for helpful discussions. This work was supported in part by the Office of Health and Environmental Research of the U.S. Department of Energy under Contract No. DE-AC03-76SF00098 and in part by the National Institutes of Health, National Heart, Lung, and Blood Institute under grant No. P01 dL25840-03.

TABLE 3. Photopeak width vs gamma ray energy at -150°C and $\tau \sim 10$ μsec using the set-up of Figure 4.

Source	γ-ray energy	photopeak amplitude[a]	photopeak FWHM[b]
^{22}Na	511 keV	5,400 e^-	9.4%
^{137}Cs	662 keV	7,040 e^-	7.2%
^{22}Na	1275 keV	13,400 e^-	5.4%
^{60}Co	1332 keV	14,100 e^-	5.3%

[a]Collected by charge amplifier
[b]Full-width at half-maximum

REFERENCES

1. Bergström, M., Bohm, C., Ericson, K., Eriksson, L., and Litton, J. (1980): Corrections for attenuation, scattered radiation and random coincidences in a ring detector positron emission transaxial tomograph. IEEE Trans. Nucl. Sci. NS-27: No. 1, 549-554.

2. Brooks, R.A., Sank, V.J., Friauf, W.S., Leighton, S.B., Cascio, H.E, and DiChiro, G. (1981): Design considerations for positron emission tomography. IEEE Trans. Biomed. Eng. BME-28: No. 2, 158-177.

3. Budinger, T.F., Derenzo, S.E., Huesman, R.H. and Cahoon, J.L. (1982): Medical criteria for the design of a dynamic positron tomograph for heart studies. IEEE Trans. Nucl. Sci. NS-29: No. 1, 488-492.

4. Ca ll, L.R., Hendry, G.O., and Currin, J.D. (1980): Design criteria fo. ulti-slice positron emission-computed tomography detector systems. IEEE Trans. Nucl. Sci. NS-27: No. 1, 485-488.

5. Derenzo, S.E. (1980): Method for optimizing side shielding in positron emission tomographs and for comparing detector materials. J. Nucl. Med. 21: 971-977.

6. Derenzo, S.E., Budinger, T.F., Huesman, R.H., and Cahoon, J.L. (1982): Dynamic positron emission tomography in man using small bismuth germanate crystals. In: Proceedings of the Sixth International Conference on Positron Annihilation, edited by P.G. Coleman, S.C. Sharma, and L.M. Diana, pp 935-945. North-Holland, New York.

7. Hoffman, E.J., Phelps, M.E., Huang, S.C., Plummer, D., and Kuhl, D.E. (1982): Evaluating the performance of multiplane positron tomographs designed for brain imaging. IEEE Trans. Nucl. Sci. NS-29: No. 1, 469-473.

8. Cho Z.H., Chan J.K., Eriksson L., Singh M., Graham S., MacDonald N.S., and Yano Y. (1975): Positron ranges obtained from biomedically important positron-emitting radionuclides. J. Nucl. Med. 16: 1174-1176.

9. Phelps, M.E., Hoffman, E.J., Huang, S.C., and Ter-Pogossian, M.M. (1975): Effect of positron range on spatial resolution. J. Nucl. Med. 16: 649-652.

10. Derenzo, S. (1979): Precision measurement of annihilation point spread distributions for medically important positron emitters. In: Positron Annihilation, edited by R.R. Hasiguti and K. Fujiwara, pp 819-823. The Japan Institute of Metals, Sendai, Japan.

11. Colombino, P., Fiscella, B., and Trossi, L. (1965): Study of positronium in water and ice from 22 to -144 °C by annihilation quantum measurements. Nuovo Cimento 38: 707-723.

12. Bohm, C., Eriksson, L., Bergström, M., Litton, J., Sudman, R., and Singh, M. (1978): A computer assisted ring detector positron camera system for reconstruction tomography of the brain. IEEE Trans. Nucl. Sci. NS-25: No. 1, 624-637.

13. Brooks, R.A., Sank, V.J., Talbert, A.J., and DiChiro, G. (1979) Sampling requirements and detector motion for positron emission tomography. IEEE Trans. Nucl. Sci. NS-26: No. 2, 2760-2763.

14. Herman, G.T. (1979): The mathematics of wobbling a ring of positron annihilation detectors. IEEE Trans. Nucl. Sci. NS-26: No. 2, 2756-2759.

15. Huesman, R.H., Derenzo, S.E., and Budinger, T.F. (1982): A two-position sampling scheme for positron emission tomography. In: Proceedings of the Third World Congress of Nuclear Medicine & Biology, edited by C. Raynaud, pp 542-545. Pergamon Press, Paris.

16. Derenzo, S.E. (1981): Monte Carlo calculations of the detection efficiency of arrays of NaI(Tl), BGO, CsF, Ge, and plastic detectors for 511 keV photons. IEEE Trans. Nucl. Sci. NS-28: No. 1, 131-136.

17. Budinger, T.F., Gullberg, G.T., and Huesman, R.H. (1979): Emission computed tomography. In: Topics in Applied Physics, Vol. 32: Image Reconstruction from Projections; Implementation and Applications, edited by G.T. Herman, pp 147-246. Springer-Verlag, Berlin.

18. Persyk, D.E., Morales, J., McKeighen, R., and Muehllehner, G. (1979): The quadrant photomultiplier. IEEE Trans Nucl Sci NS-26: No. 1, 364-367.

19. Uchida, H., Yamashita, Y., Yamashita, T., and Hayashi, T. (1983): Advantageous use of new dual rectangular photomultiplier for positron CT. IEEE Trans. Nucl. Sci. NS-30: No. 1, 451-454.

20. Burnham, C., Bradshaw, J., Kaufman, D., Chesler, D., and Brownell, G.L. (1983): A positron tomograph employing a one dimension BGO scintillation camera. IEEE Trans. Nucl. Sci. NS-30: No. 1, 661-664.

21. Eriksson, L. (1983): A high resolution positron camera. In: Proceedings of the VII Nobel Conference: "The Metabolism of the Human Brain Studied with Positron Emission Tomography", edited by L. Widén, (in press). Karolinska Institute, Stockholm.

22. Murayama, H., Nohara, N., Tanaka, E., and Tayashi, T. (1982): A quad BGO detector and its timing and positioning discrimination for positron computed tomography. Nucl. Instr. Meth. 192: 501-511.

23. Barton, J.B., Hoffman, E.J., Iwanczyk, J.S., Dabrowski, A.J., and Kusmiss, J.H. (1983): A high-resolution detection system for positron tomography. IEEE Trans. Nucl. Sci. NS-30: No. 1, 671-675.

24. Derenzo, S.E. (1983): Gamma-ray spectroscopy using small, cooled bismuth germanate scintillators and silicon photodiodes. Nucl. Instr. Meth., (in press).

25. N. Mullani, (1982), private communication.

26. Derenzo, S.E. and Riles, J. (1982): Monte Carlo calculations of the optical coupling between bismuth germanate crystals and photomultiplier tubes. IEEE Trans. Nucl. Sci. NS-29: No. 1, 191-195.

27. Blanar, G., Dietl, H., Dobbins, J., Eigen, G., Lorenz, E., Pauss, F., Pimpl, W., Vogel, H., and Weissbach, P. (1982): Photodiode readout for scintillating crystals of BGO and NaI(Tl). Nucl. Instr. Meth. 203: 213-221.

28. Groom, D.E. (1982): Silicon photodiode detection of bismuth germanate scintillation light. In: International Workshop on Bismuth Germanate, edited by D.G. Coyne, pp 256-265. Princeton University, Princeton.

29. Iwanczyk, J.S., Barton, J.B., Dabrowski, A.J., Kusmiss, J.H., and Szymczyk, W.M. (1983): A novel radiation detector consisting of an HgI_2 photodetector coupled to a scintillator. IEEE Trans. Nucl. Sci. NS-30: No. 1, 363-367.